Article

Structural, Optoelectrical, Linear, and Nonlinear Optical Characterizations of Dip-Synthesized Undoped ZnO and Group III Elements (B, Al, Ga, and In)-Doped ZnO Thin Films

A. M. Alsaad [1,*], A. A. Ahmad [1], I. A. Qattan [2], Qais M. Al-Bataineh [1] and Zaid Albataineh [3]

[1] Department of Physical Sciences, Jordan University of Science & Technology, P.O. Box 3030, Irbid-22110, Jordan; sema_just@yahoo.com (A.A.A.); qalbataineh@ymail.com (Q.M.A.-B.)
[2] Department of Physics, Khalifa University of Science and Technology, P.O. Box 127788, Abu Dhabi, UAE; issam.qattan@kustar.ac.ae
[3] Department of Electronic Engineering, Yarmouk University, Irbid 21163, Jordan; zaid.bataineh@yu.edu.jo
* Correspondence: alsaad11@just.edu.jo or amalsaad@unomaha.edu; Tel.: +962-791314650 or +962-7201000/23422; Fax: +962-2-7201071

Received: 13 February 2020; Accepted: 18 March 2020; Published: 27 March 2020

Abstract: Undoped ZnO and group III (B, Al, Ga, and In)-doped ZnO thin films at 3% doping concentration level are dip-coated on glass substrates using a sol-gel technique. The optical properties of the as-prepared thin films are investigated using UV–Vis spectrophotometer measurements. Transmittance of all investigated thin films is found to attain high values of ≥80% in the visible region. We found that the index of refraction of undoped ZnO films exhibits values ranging between 1.6 and 2.2 and approximately match that of bulk ZnO. Furthermore, we measure and interpret nonlinear optical parameters and the electrical and optical conductivities of the investigated thin films to obtain a deeper insight from fundamental and practical points of view. In addition, the structural properties of all studied thin film samples are investigated using the XRD technique. In particular, undoped ZnO thin film is found to exhibit a hexagonal structure. Due to the large difference in size of boron and indium compared with that of zinc, doping ZnO thin films with these two elements is expected to cause a phase transition. However, Al-doped ZnO and Ga-doped ZnO thin films preserve the hexagonal phase. Moreover, as boron and indium are introduced in ZnO thin films, the grain size increases. On the other hand, grain size is found to decrease upon doping ZnO with aluminum and gallium. The drastic enhancement of optical properties of annealed dip-synthesized undoped ZnO thin films upon doping with group III metals paves the way to tune these properties in a skillful manner, in order to be used as key candidate materials in the fabrication of modern optoelectronic devices.

Keywords: thin films; undoped Zinc oxide (ZnO); boron-doped ZnO; aluminum-doped ZnO; gallium-doped ZnO; indium-doped ZnO; dopant material; sol gel; structural properties; optical properties; nonlinear optical properties

---

1. Introduction

In the past two decades, the synthesis, design, and characterization of III-V and II-VI semiconductors have fascinated several research groups around the globe. II-oxides have gained a lot of thrust. In particular, ZnO is considered to be a very important semiconductor material due to its fundamental and physical properties. It has been reported and implemented as a key candidate material for potential applications in optoelectronic devices, photovoltaic devices, gas sensors, light

emitting diodes, and pharmaceutical applications [1–5]. ZnO has been the focal point of much recent research because it possesses certain characteristics that make it a very interesting material from both fundamental and practical points of view. The n-type ZnO semiconductor exhibits several interesting features, such as its room temperature direct wide band-gap of 3.37 eV, which enables it to be used for a wide range of optical applications [6]. Additionally, it is unusual for ZnO to have an exciton binding energy of 60 meV. This large value is very interesting, as it is useful for the development of many optoelectronic devices. Specifically, in the photoluminescent spectrum of ZnO, very sharp emission peaks are observed, due to excitonic radiative recombination processes. These types of emissions have many possible applications, such as UV excitonic lasers, tunable UV photodetectors, and light emitting diodes. Furthermore, other excitonic peaks observed can be distinguished depending on their emission energy. Therefore, it is possible to observe and differentiate free excitons from bound excitons, as well as bulk exitonic processes from surface excitonic processes [7]. Interestingly, ZnO has been found to exhibit high room temperature carrier mobility (200 cm^2 V^{-1} s^{-1} for single crystals) and found to be thermally very stable [8]. It has been reported that ZnO demonstrates fairly good pyro-electricity and piezoelectricity features [9]. Moreover, ZnO has good transparency in the visible range spectrum and large electrical conductivity [10,11].

ZnO thin films are conventionally doped and co-doped with a number of proper dopants to improve their optical and electrical properties [12]. In principle, we investigate the optical and structural properties of sol-gel dip-synthesized group III (B, Al, Ga, and In)-doped ZnO thin films in this current work. The structural, transport, and optical properties of B-doped ZnO, Al-doped ZnO, Ga-doped ZnO, and In-doped ZnO thin films are found to exhibit different properties than un-doped ZnO thin films [8,12–20]. Deposition of undoped ZnO and group III (B, Al, Ga, and In)-doped ZnO thin films can be achieved by using techniques such chemical vapor deposition [2,21], magnetron sputtering [15,22], pulse laser deposition [23], electrochemical deposition [24], and the sol-gel method [14,25].

Undoped ZnO and group III (B, Al, Ga, and In)-doped ZnO thin films at a doping concentration level of 3% are deposited on a glass substrate by employing the sol-gel dip-coating technique. The effect of introducing four elements from group III onto the structural and optical properties of ZnO thin films is investigated, analyzed, and interpreted. The X-ray diffraction (XRD) technique is used to investigate the structure of ZnO thin films. The optical response of thin films is characterized by measuring the transmittance and reflectance using a double beam UV-Vis pectrophotometer (model U-3900H).

2. Experimental Procedure

2.1. Preparation of Undoped ZnO Solution

The procedure to prepare the sol-gel solution of ZnO is as follows: We start by dissolving 4.38 g of zinc acetate dihydrated ($Zn(CH_3CO_2)_2$ $2H_2O$, purity of 99.5%) in 50 mL absolute ethanol (purity of 99.85%) at room temperature, using a magnetic stirrer operating at a rate of 600 revolutions per minute for 50 min. Consecutively, 1.7 mL of mono-ethanolamine stabilizer is added dropwise to the gel solution while maintaining continuous stirring of the mixture until it acquired high transparency. The resulting mixture was additionally stirred for 40 min to ensure that a homogeneous transparent solution is obtained. Finally, the mixture is filtrated by using the standard 0.45 µm filter paper [26,27].

2.2. Preparation of Group III Elements-Doped ZnO Solutions

The synthesized doped ZnO solutions, mainly, B-doped ZnO, Al-doped ZnO, Ga-doped ZnO, and In-doped ZnO solutions, are obtained from the well-prepared ZnO solution by implementing the sol-gel technique. The boric acid (H_3BO_3), aluminum nitrate (Al $(NO_3)3$ $9H_2O$), gallium nitrate (Ga $(NO_3)_2$), and indium chloride ($InCl_3$) are added in a 3% ratio to the ZnO solution. The miscellaneous highly transparent solution for each of the doped systems is obtained by magnetically stirring it for 30–40 min at a specific temperature. Finally, the resulting solution is filtrated by 0.45 µm filter paper [27–29].

This procedure is followed strictly to ensure the creation of solutions that can maintain a high degree of transparency.

2.3. Preparation of Undoped ZnO and Group III Elements-ZnO Thin Films

Having prepared the solution with the desired properties, the substrate is then dipped in the solution for 2 h using the dip-coating technique. Using this technique, it is possible to get thin films of an average thickness of 500 nm. The resulting films are then dried in oven for 15 min at 120 °C to evaporate the solvent and the contaminated organic residues. In order to obtain un-doped ZnO and group III (B, Al, Ga, and In)-doped ZnO thin films with the best possible crystalline structure, all films are annealed in air at 500 °C for 2 h [26,27].

2.4. Characterization of Undoped ZnO and Group III Elements-ZnO Thin Films

Material characterization and device performance modeling are typically investigated by analytical expressions for the optical functions of semiconductors and dielectric thin films [30]. Experimentally, a double-beam UV-Vis spectrophotometer (U-3900H, LABINDIA, Mumbai, India) in the wavelength range of 250−700 nm is used to investigate the optical properties of thin films by measuring the transmittance and the reflectance. Real and imaginary parts of the dielectric functions (ε_1 and ε_2) or the complex refractive index (n and k), absorption coefficient (α), and optical band gap energy can be calculated using transmittance and reflectance spectra and by the determination of film thickness [31–34].

Powder X-ray diffraction experiments were performed using X-Ray diffraction (Rigaku Ultima IV) at Jordan University of Science and Technology, Pharmaceutical Research Center. The thicknesses of the undoped ZnO and group III elements-ZnO thin films on glass are determined using scanning electron microscopy (SEM, Quanta FEG 450) at Jordan University of Science and Technology, Nanotechnology Institute. The films' thickness is estimated to be 500 nm on average. Thin film surfaces morphology and dispensability are investigated using scanning electron microscopy (SEM, Quanta FEG 450) at Jordan University of Science and Technology, Nanotechnology Institute.

3. Results and Discussion

3.1. UV-Vis Spectroscopy

The optical properties of undoped ZnO and group III (B, Al, Ga, and In)-doped ZnO thin films at 3% doping level are explored by measuring and analyzing the transmittance $T\%(\lambda)$ and reflectance $R\%(\lambda)$ spectra in the spectral range of 250−800 nm to obtain a deeper insight into the optoelectronic nature and potential applications of the films [35]. It is worth mentioning that several factors may affect the optical properties, such as the preparation technique, synthesis conditions, surface morphology, dopants, and interaction of films with the surrounding environment [36]. Figure 1a shows the transmittance of thin film samples investigated in this work. The figure indicates that all fabricated films are transparent in the visible range ($T\% > 70\%$). The wavelengths at which absorption edges of Al-doped ZnO and Ga-doped ZnO occur are smaller than the wavelength at which absorption edge of undoped ZnO takes place. On the other hand, absorption edges of B-doped ZnO and In-doped ZnO are located at wavelengths greater than that of the absorption edge of un-doped ZnO thin films. It can be clearly seen that transmittance beyond the absorption edge of un-doped ZnO has values ranging between 80% and 90%. B-doped ZnO, Al-doped ZnO, and Ga-doped ZnO thin films are found to have transmittance values close to that of undoped ZnO, which is in agreement with our previous published work on B-doped ZnO thin films [27]. The measured transmittance of Al-doped ZnO thin films is in good agreement with the findings reported in [16,20]. The obtained transmittance of Ga-doped ZnO thin films is consistent with previously reported findings [18,37]. The transmittance $T\%(\lambda)$ of In-doped ZnO thin films is found to decrease to 70–80%, very close to the values reported by similar previous studies [8,19,38]. Inspecting Figure 1a carefully shows that transmittance of undoped ZnO

and group III elements (B, Al, Ga and In)-doped ZnO thin films demonstrate a continuous decrease in transmittance as the photon energy striking the samples increases. This decrease can be interpreted in terms of the enhancement of the charge carriers in a relatively weak crystal structure when energetic photons are occurring [39]. Thus, transmittance values could provide a way to unveil the details of thin film structure.

Optical absorption studies provide details of the electronic states in the high energy part of the optical absorption spectrum and the atomic vibrations in the low energy part of the spectrum. The information obtained from optical spectra can be directly correlated to determine band gap energy E_g and to explain the band structure of semiconductors and non-metallic materials [40–42]. The Tauc model is used to extrapolate E_g of thin films. A Tauc plot is obtained by plotting the photon's incident energy (hv) in eV against $(\alpha hv)^2$ of the direct transition of ZnO thin films, where α is the absorption coefficient given by $\alpha = (1/d)\, ln(1/T)$ and d is the film thickness ($d = 500$ nm). Figure 2b shows the Tauc plot of undoped ZnO and group III (B, Al, Ga, and In)-doped ZnO thin films. The E_g values are measured by extrapolating the linear part of the relationship to the incident photon energy at which E_g equals the incident photon energy (hv). The E_g of undoped ZnO is found to be 3.270 eV, which is in excellent agreement with previous studies [27,29]. The E_g of the B-doped ZnO thin film is found to decrease to 3.161 eV, which is consistent with previous works [27,29]. A further decrease of E_g to 3.093 eV takes place as gallium is introduced into ZnO thin films in good agreement with [37]. On the other hand, the E_g of the In-doped ZnO thin film is found to increase to 3.314 eV, a value that agrees well with the findings of [8], and to 3.369 eV when aluminum is introduced into the ZnO thin films, which is in excellent agreement with reported values of [16,17]. The fluctuations in the values of E_g of doped ZnO thin films are expected and can be explained in terms of the variations in the values of crystallite sizes as the dopants are introduced in ZnO thin films, as will be demonstrated later by the X-ray diffraction patterns. In addition, the existence of the dopant levels in the band gap allows the transition of electrons from the top of the valance band to the doping energy levels in the band gap and vice versa. The E_g of a thin film is defined traditionally in terms of an effective sub-band gap between the valence band and the conduction band, and therefore it may be drastically influenced by the presence of aggregation and clusters formed by dopant atoms in thin films. In order to investigate sub-band gaps in thin films, we use what is called the Urbach energy, or E_U method [41,43–46]. According to this method, near the optical band edge, the relationship between (α) and (hv), known as the Urbach empirical rule, can be expressed as $\alpha = \alpha_0 \exp(hv/E_U)$, where α_0 is a constant, h_v is the incident photon energy, and E_u is the Urbach energy. By plotting the dependence of $\ln(\alpha)$ versus hv, it is possible to determine E_U. The E_g values and the band tail width are tabulated in Table 1. The positions of the conduction and valence bands of a thin film at a given doping level can be determined if the electron affinity energy and the ionization energy of its constituents are known. For undoped ZnO and group III elements (B, Al, Ga and In)-doped ZnO thin films at 3% doping level, these positions can be calculated as [47,48],

$$E_g E_{CB} = X - E_e - 0.5 \quad (1)$$

where:

$$X = \left[\left(X_{Z1}^{x_1}\right) * \left(X_{Z2}^{x_2}\right) * \ldots\right]^{(1/(x_1+x_2+\cdots)} \quad (2)$$

and

$$X_Z = \left(\frac{1}{2}\right)\left(E_{EA}^{Z} + E_{Ion}^{Z}\right) \quad (3)$$

where E_{CB} is the conduction band energy and E_e is the energy of free electrons of the hydrogen scale equal to 4.5 eV [47]. The parameter X is an energy parameter that depends on the elements used in the thin film. E_{EA}^{Z} is the electron affinity energy and E_{Ion}^{Z} is the ionization energy of the Z elements. The electron affinity is defined as the energy obtained by moving an electron from the vacuum just outside the semiconductor to the bottom of the conduction band just inside the semiconductor,

i.e., $E_{EA} = E_{VB} - E_{CB}$. The calculated values of the energy parameter (X), the conduction band potential (E_{CB}), and the positions of both the conduction and the valence bands of undoped ZnO and group III elements (B, Al, Ga and In)-doped ZnO thin films at doping level of 3% are presented in Table 1 and sketched on a schematic energy diagram as shown in Figure 1c. Careful inspection of Figure 1c indicates that the positions of the conduction band minimum (CBM) of B-doped ZnO, Al-doped ZnO, and Ga-doped ZnO thin films are located at −0.175 eV, −0.331 eV, −0.191 eV, and −0.307 eV inside the conduction band, respectively. This means that CBMs of these thin films are shifted toward higher negative energy regions with respect to the CBM of the undoped ZnO thin films located at −0.172 eV. Furthermore, the valence band maximum (VBMs) of B-doped ZnO, Al-doped ZnO and Ga-doped ZnO thin films are found to be located at 2.985 eV, 3.039 eV, 2.899 eV, and 3.003 eV, respectively. This clearly shows that the VBMs of these films are shifted toward less positive energy regions of the valence band with respect to the VBM of the undoped ZnO thin film located at 3.098 eV. This indicates that values of band gap of doped ZnO thin films are largely tuned and engineered by controlling the type of the dopant and the doping level. Figure 1c elucidates the defect bands shaped as transitional states in the band gap of the material. These defect band states generate a sub-band gap spreading from the lower level of the conduction band to deep down in the band gap. Likewise, the defect states very near to the valence band also smudge the valence band edge deep inside the gap. Therefore, on both sides of the VBM and CBM, a sub-band gap is formed. This defect sub-band gap is known as the Urbach tail, and the energy associated with this defect tail is referred to as Urbach energy.

Table 1. The band gap energy E_{gap}, Urbach energy E_{U}, the energy parameter (X), and the positions of both the conduction and valence bands of undoped ZnO and group III elements (B, Al, Ga and In)-doped ZnO thin films at a doping level of 3%. BZO, AZO, GZO, and IZO stands for B-doped ZnO, Al-doped ZnO, Ga-doped ZnO, and In-doped ZnO thin films, respectively.

Sample	E_{gap} (eV)	E_U (eV)	X (ZnO) (eV)	X (Z) (eV)	X (tot) (eV)	E_{CB} (eV)	E_{VB} (eV)
ZnO	3.270	0.169	5.963	0.000	5.963	−0.172	3.098
BZO	3.161	0.150	5.963	4.286	5.905	−0.175	2.985
AZO	3.369	0.301	5.963	3.224	5.854	−0.331	3.039
GZO	3.093	0.131	5.963	3.218	5.854	−0.191	2.899
IZO	3.314	0.384	5.963	3.104	5.848	−0.307	3.003

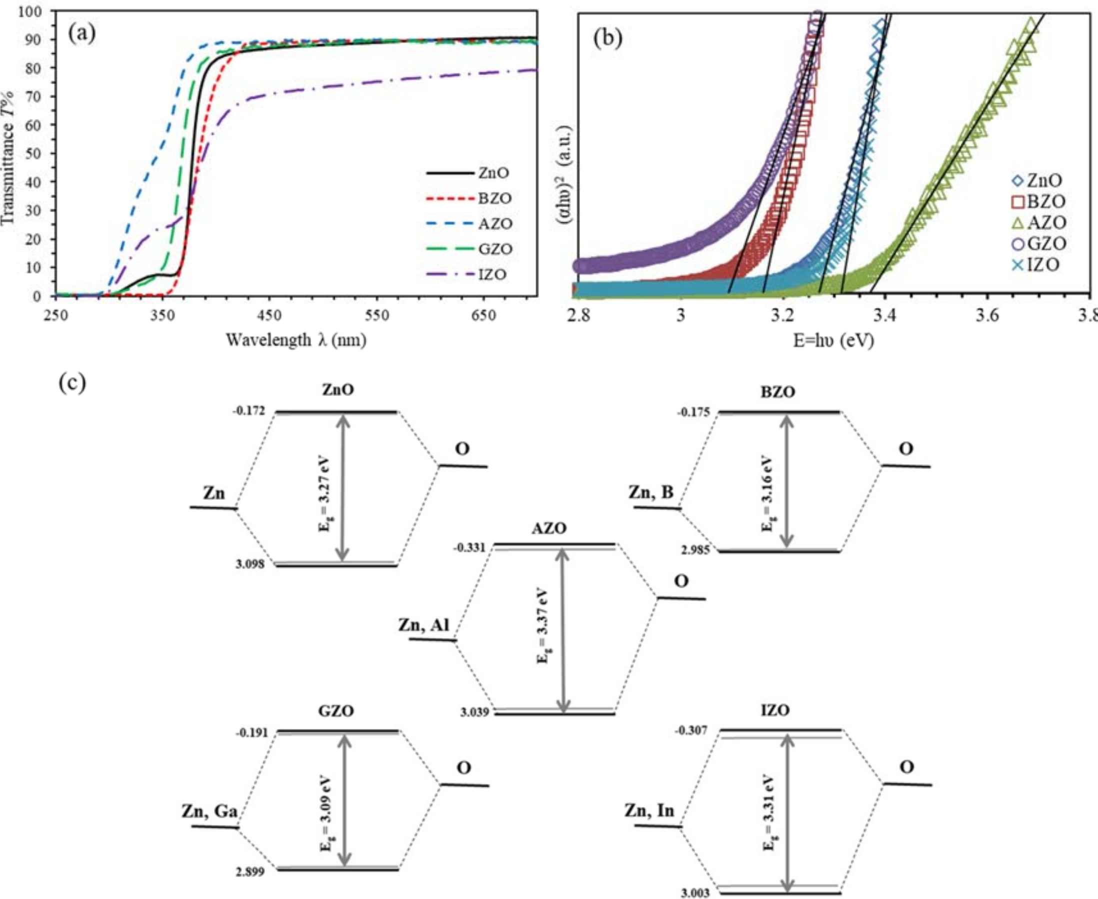

Figure 1. (**a**) Transmittance spectra, (**b**) band gap energy, and (**c**) schematic images and binding structures of undoped ZnO and group III elements (B, Al, Ga and In)-doped ZnO thin films at a doping level of 3%.

The value of the reflectance is measured by spectrophotometer with a total internal reflectance sphere. Analysis of the reflectance spectra show that they exhibit a reverse behavior to that of the transmittance, as shown in Figure 2a. The values of reflectance of undoped ZnO thin films are found to be in the range of 5–10%, as the wavelength decreases from 700 nm to 350 nm. As can be easily seen from Figure 2a, the reflectance of In-doped ZnO and B-doped ZnO thin films exhibit higher values than that of undoped ZnO in the same spectral range. On the other hand, Al-doped ZnO and Ga-doped ZnO display lower reflectance than that of undoped ZnO. Measuring the complex refractive index N is crucial to get a deeper insight into the optical properties of thin films. Thin film applications such as fabrication of any optical devices, e.g., switches, filters, modulation, etc. [35], requires precise measurement of N that can be decomposed into a real part called the index of refraction (n) and an imaginary part called the extinction coefficient (k); $N = n + ik$. The parameter n can be calculated as $n = (1 + R/1 - R) + \sqrt{\left(4R/(1-R)^2\right) - k^2}$ [27]. We measure n as a function of the wavelength of incident light as shown in Figure 2b, n of the undoped ZnO thin film is found to exhibit values between 1.5 and 2.0 as the wavelength of incident photon decreases from 700 nm to 350 nm. In addition, Al-doped ZnO and Ga-doped ZnO thin films are found to exhibit values lower than that of undoped ZnO thin films. On the contrary, In-doped ZnO and B-doped ZnO thin films are found to adopt values higher than that of the undoped ZnO thin films. Consequently, optical properties of ZnO thin films can be significantly manipulated by controlling the type of the dopants and the level of doping.

The amount of light energy loss by absorption and scattering in the thin films is fundamentally estimated by measuring the extinction coefficient. The extinction coefficient (k) depends on the density of free electrons and the structural defects in the thin films. k can be expressed as, $k = \alpha\lambda/4\pi$ [27].

Figure 2c shows the values of k as a function of the wavelength of incident light. Clearly, B-doped ZnO, Al-doped ZnO, and Ga-doped ZnO are found to exhibit values very close to that of undoped ZnO thin films. Exceptionally, In-doped ZnO thin film is found to exhibit larger k values than that of undoped ZnO thin films.

Next, skin or penetration depth (δ) that denotes the thickness of thin films at which interior optical photon density decays to 1/α of the value at the surface is calculated [35,49]. The parameter δ is related to the absorption coefficient (α) by the relation $\delta = 1/\alpha$ [49]. Figure 2d shows δ as a function of the incident photon energy (hv) for all thin film samples investigated in this work. It can be easily demonstrated that δ of all studied thin films decreases as the photon energy increases. For wavelengths greater than the cutoff wavelength ($\lambda = 390$ nm or $hv = 3.6$ eV), the absorption effect vanishes and the amplitude vanishes as light penetrates large distances.

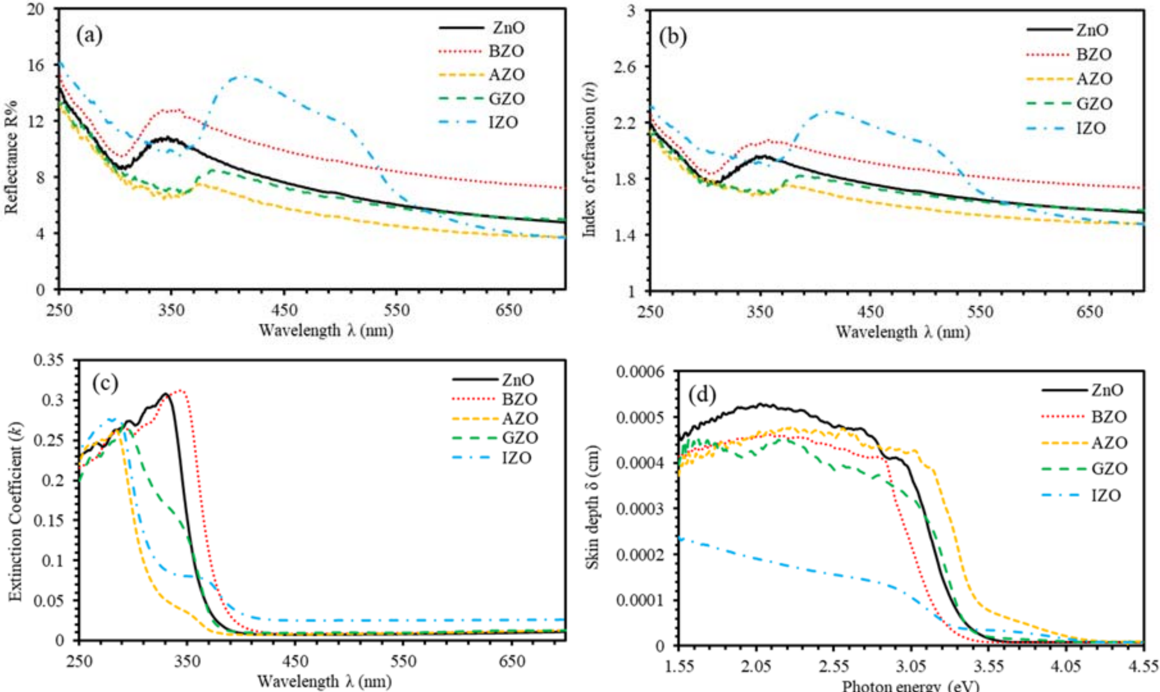

Figure 2. (**a**) Reflectance spectra, (**b**) index of refraction spectra (n), (**c**) extinction coefficient spectra (k), and (**d**) dependence of the skin depth on the photon energy of undoped ZnO and group III elements (B, Al, Ga, and In)-doped ZnO thin films at 3% doping concentration.

3.2. Dispersion of Refractive Index

Dispersion parameters of undoped ZnO and group III elements (B, Al, Ga, and In)-doped ZnO thin films at 3% doping concentration are calculated using the Wemple–DiDomenico (WDD) single-oscillator model that relates different optical parameters of thin films [50,51],

$$n^2 - 1 = \frac{E_d E_0}{E_0^2 - E^2} \tag{4}$$

where E_d denotes the dispersion energy. It is related to the iconicity, anion valency, and coordination number of the material. E_0 denotes the single oscillator energy and n represents the refractive index. The single effective oscillator equation is used for fitting the experimental data due to its easiness in providing an intuitive physical interpretation of the measured quantities [52]. By plotting $\left(n^2 - 1\right)^{-1}$ versus $(hv)^2$, the dispersion parameters of undoped ZnO and group III elements (B, Al, Ga, and In)-doped ZnO thin films at 3% doping concentration can be evaluated by fitting a straight line.

The values of E_0 and E_d can then be calculated from the slope $(E_0 E_d)^{-1}$ which intercepts on the vertical axis (E_0/E_d). The values of E_d and E_0 are presented in Table 2. Clearly, E_0 of Al-doped ZnO and In-doped ZnO thin films exhibit values that are slightly smaller than that of undoped ZnO thin films. This could be attributed to the reduction of energy and iconicity of the bonds formed between the film elements. However, B-doped ZnO and Ga-doped ZnO thin films exhibit higher values. This could be interpreted in terms of increasing the energy and iconicity of the bonds [35]. Having estimated the values of E_0 and E_d, we then determine the zero-frequency dielectric constant ε_0 and zero-frequency refractive index n_0 by rewriting Equation (4) and put $hv = 0$, giving:

$$\varepsilon_0 = n_0^2 = 1 + \frac{E_d}{E_0} \tag{5}$$

The calculated values of zero-frequency dielectric constant ε_0 and zero-frequency refractive index n_0 of all thin film samples are presented in Table 2. Values of n_0 are found to be in good agreement with theoretical and experimental values of the normal refractive index. In addition, values ε_0 of and n_0 of undoped ZnO thin films are found to be 2.357 and 1.535, respectively. Careful inspection of Table 2 indicates that B-doped ZnO and In-doped ZnO thin films exhibit higher values of ε_0 and n_0, whereas Al-doped ZnO and Ga-doped ZnO thin films exhibit smaller values of ε_0 and n_0 than those of un-doped ZnO thin films.

3.3. Nonlinear Optical Properties

The nonlinear optical parameters of thin films, such as third-order nonlinear susceptibility $\chi^{(3)}$ and nonlinear refractive index n_2, are crucial for the fabrication of several electronic and photonic devices [53,54]. The n_2 and $\chi^{(3)}$ parameters are calculated by combining Miller's generalized rule and the parameters from the WDD single oscillator model [55–57] by utilizing the following formulas [58–62],

$$\chi^{(3)} = 6.82 * 10^{-15} (E_d/E_0)^4 \ (esu) \tag{6}$$

$$n_2 = \frac{12\pi\chi^{(3)}}{n_0} \tag{7}$$

The obtained $\chi^{(3)}$ and n_2 values are presented in Table 2. Both $\chi^{(3)}$ and n_2 and the index of refraction parameters are found to adopt similar behaviors.

Table 2. Estimation of some essential optoelectronic parameters of undoped ZnO and group III elements (B, Al, Ga, and In)-doped ZnO thin films at 3% doping concentration.

Parameter	ZnO	BZO	AZO	GZO	IZO
Effective single oscillator, E_0 (eV)	4.616	5.015	4.609	4.732	4.011
Dispersion energy, E_d (eV)	6.261	9.362	4.976	6.328	7.990
Zero-frequency refractive index, n_0	1.535	1.693	1.442	1.529	1.729
Zero-frequency dielectric constant, ε_0	2.357	2.867	2.080	2.337	2.992
Optical oscillator strengths $f\left(\mathrm{eV}^2\right)$	28.902	46.948	22.936	29.940	32.051
Linear optical susceptibility, $\chi^{(1)}$	0.108	0.149	0.086	0.106	0.159
Third-order nonlinear optical susceptibility, $\chi^{(3)} \times 10^{-14}$ (esu)	2.309	8.287	9.264	2.181	1.074
The nonlinear refractive index, $n_2 \times 10^{-13}$	5.668	1.844	2.421	5.375	2.339

3.4. Optical and Electrical Conductivities

Non-linear optical properties, as well as optical and electrical conductivities σ_{opt} and σ_{ele} are measured to obtain a deeper insight into the possible potential optical, optoelectronic, and optoelectrical applications of dip-synthesized undoped ZnO and group III Elements (B, Al, Ga, and In)-doped ZnO thin films. The σ_{opt} and σ_{ele} can be regarded as functions of current density and electric field for certain frequencies and therefore both depend strongly on the optical band gap of the nanocomposite. σ_{opt} and σ_{ele} could be expressed as $\sigma_{opt} = \alpha nc/4\pi$ and $\sigma_{ele} = 2\lambda\sigma_{opt}/\alpha$ [53,54,63,64], where c is the speed of light in air or free space. Figure 3a shows the σ_{opt} spectra of undoped ZnO and group III elements (B, Al, Ga, and In)-doped ZnO thin films at 3% doping concentration. The significant increase of σ_{opt} as the photon energy increases is due to the high absorbent nature of thin films in the high frequency region and may be due to the excitation of electrons by the energetic photons. Moreover, the dependence of σ_{ele} on the photon energy of all investigated thin films are depicted in Figure 3b. Our results regarding σ_{ele} show that for all investigated thin films, it decreases as photon energy is increased. In addition, B-doped ZnO and In-doped ZnO thin films demonstrate σ_{ele} values higher than that of undoped ZnO, whereas Al-doped ZnO and Ga-doped ZnO display lower values.

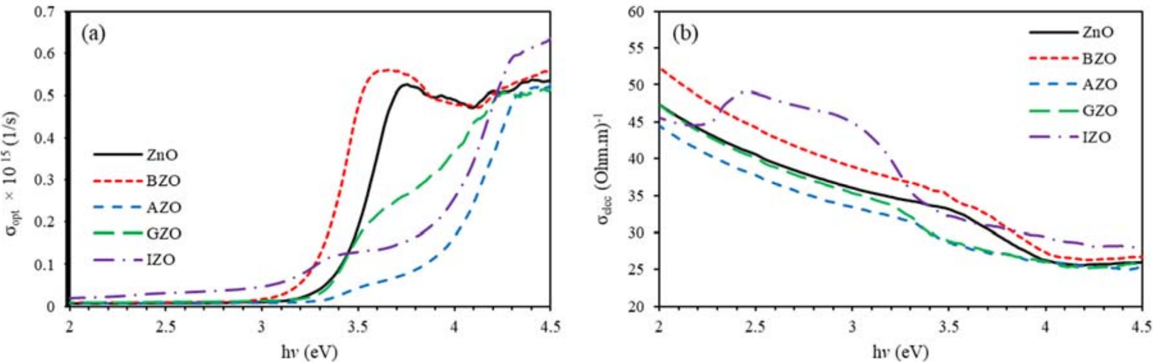

Figure 3. (**a**) The variation of the optical conductivity with the photon energy, and (**b**) the variation of the electrical conductivity with the photon energy of undoped ZnO and group III elements (B, Al, Ga, and In)-doped ZnO thin films at 3% doping concentration.

3.5. X-Ray Diffraction Analysis

Crystallinity of all investigated thin films is investigated by a powder X-Ray data analysis system [65], using a Cu$K\alpha$ ray with a wavelength of 0.1540598 nm. Figure 4 shows the X-ray diffraction (XRD) patterns of all thin film samples. The measured XRD patterns are found to demonstrate peaks observed at Bragg's angles of 32.08°, 34.80°′ and 36.62°, corresponding to (100), (002), and (101) crystallographic planer orientations, respectively. The XRD patterns show a large difference between the angular positions of group III elements (B, Al, Ga, and In)-doped ZnO thin films and those of undoped ZnO thin films. This can be attributed to the large lattice mismatch induced by the large difference between the lattice parameters of dopant atoms and that of the ZnO host. The lattice mismatch induces large mechanical stress. Clearly, the (002) crystallographic orientation plane dominantly determines the polycrystalline features of undoped ZnO thin films. The XRD patterns reported in this work are consistent with those reported in [14]. The pioneering study [66] reported that the (002) crystallographic orientation of ZnO thin films seems to be preferred by amorphous substrates, such as glass. Furthermore, another study [67] investigated the preferential orientations of textured thin films along the c-axis, perpendicular to the substrate and reported results in good agreement with XRD findings of this work. Additionally, [68] attributed the preferential growth of ZnO thin films along the (002) plane to the low surface free energy of this plane. Interestingly, the intensity of the peak associated with the (002) crystallographic plane in XRD patterns increases steadily, thus enhancing crystallinity of ZnO thin films as the annealing temperature is increased, which is consistent with

the results reported [69]. XRD patterns revealed that 3% B-doped ZnO thin films grow preferentially with a single (100) crystallographic plane, in agreement with our previous study on doped B-ZnO thin films [27]. This can likely be attributed to the large difference of atomic and ionic radii of Zn atoms (atomic and ionic radii of 142 pm and 74 pm) and B atoms (atomic and ionic radii of 87 pm and 25 pm). In addition, the XRD pattern of doped In-doped ZnO thin films shows mainly one-orientation, corresponding to (101) diffraction planes, consistent with the findings of [70]. This can be interpreted in terms of the large difference between atomic and ionic radii of Zn atoms and In atoms (atomic and ionic radii of 156 pm and 76 pm). Furthermore, Al-doped ZnO and Ga-doped ZnO thin films are found to exhibit all ZnO diffraction peaks at (100), (002), and (101) diffraction planes, in good agreement with the findings of [5,71,72] and T. Ivanova et al. [73]. In addition, XRD patterns revealed that all crystallographic orientations are shifted into small Bragg's angles, that could be explained in terms of the difference between atomic and ionic radii of Zn atoms and Al atoms (atomic and ionic radii of 118 pm and 53 pm) and Ga atoms (atomic and ionic radii of 136 pm and 61 pm).

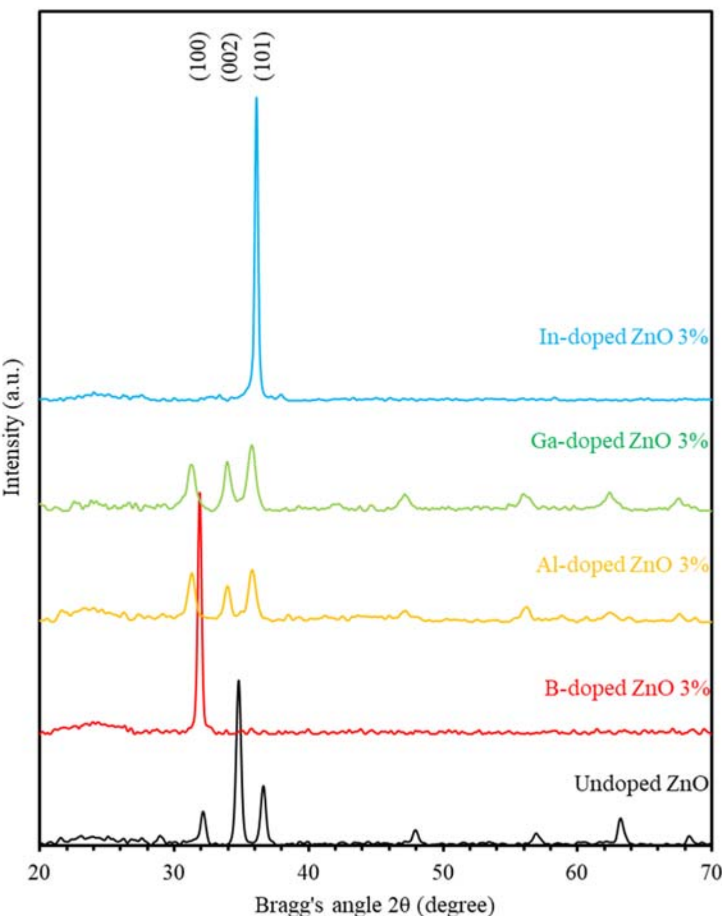

Figure 4. The X-ray diffraction patterns of undoped ZnO and group III elements (B, Al, Ga, and In)-doped ZnO thin films at 3% doping concentration.

The lattice parameters of the wurtzite microstructure of undoped ZnO thin film can be expressed as [74],

$$a = \frac{\lambda}{\sqrt{3}\sin\theta_{(100)}} \tag{8}$$

$$c = \frac{\lambda}{\sin\theta_{(002)}} \tag{9}$$

where λ is X-ray wavelength (λ = 0.1540598 nm). The lattice constants (*a* and *c*) of undoped ZnO thin films are found to be 3.227 Å and 5.171 Å, respectively, in a good agreement with those reported by the Joint Committee on Powder Diffraction Standards (JCPDS 36-1451) [74]. Due to the formation of polycrystalline aggregates, the crystallite size (*D*) of the particles is different from the particle size [75]. The *D* parameter of thin film microstructure associated with (002) crystallographic orientations is calculated using the Scherer formula, $D = k\lambda/\beta_{2\theta}\cos\theta$, where k is a constant taken to be 0.94, λ is X-ray wavelength (λ = 0.1540598nm) and $\beta_{2\theta}$ is the full width at half-maximum value (FWHM) of the peak in radians [76]. The dislocation density (δ) represents the amount of defects in the film and is estimated by $\delta = 1/D^2$ [76]. The strain (ε) and crystallite density (*N*) of thin film microstructures can be found from $\varepsilon = \beta\cot\theta/4$ and $N = t/D^3$, respectively [19,76]. Table 3 shows the structure parameters of undoped ZnO and group III elements (B, Al, Ga, and In)-doped ZnO thin films at 3% doping concentration. Careful inspection of Table 3 indicates that *D* increases upon doping with boron and indium, and decreases when aluminum and gallium are introduced as a dopant in ZnO thin films. We found that ε and *D* are inversely proportional due to the shrinkage of the space occupied by the arranged atoms inside the crystalline structure and the expansion of the total surface area [77].

Table 3. The structure parameters of undoped ZnO and group III elements (B, Al, Ga, and In)-doped ZnO thin films at 3% doping concentration.

Samples	Crystalline Size *D* (nm)	Dislocation Density δ (10^{15})	Strain ε (10^{-3})	Crystalline Density (10^{16})
ZnO	19.298	2.693	6.353	6.998
BZO	24.932	1.609	5.286	3.226
AZO	14.132	5.118	8.938	18.490
GZO	11.877	7.197	10.636	30.746
IZO	66.995	0.223	1.744	1.663

3.6. Scanning Electron Microscopy

Figure 5a–e shows the SEM micrographs of undoped ZnO, B-doped ZnO, Al-doped ZnO, Ga-doped ZnO, and In-doped ZnO, respectively. SEM micrographs of undoped ZnO thin film shows that it exhibits a flat frictionless surface with tiny grains of ZnO scattered throughout the surface, as can be seen in Figure 5a. The diameter of each single nanoparticle was estimated to be around 77 nm. SEM micrographs of B-doped ZnO thin films (Figure 5b), demonstrate the coarse characteristics pictured by unsystematically dispersed ice land-like features. SEM micrographs of Al-doped ZnO thin films (Figure 5c) demonstrate that grains become finer and clearer. Upon inspecting SEM micrographs of Ga-doped ZnO (Figure 5d), one may see that small nanoparticles appeared on the surface, which have been refined and softened to form regular nanofeatures. Finally, In-doped ZnO thin films micrographs (Figure 5e) show sheet-like features with few cracks. These results agree well with the XRD patterns, which demonstrate a decrease in the grain size of Al-doped ZnO and Ga-doped ZnO thin films, and an increase of grain size of B-doped ZnO and In-doped ZnO thin films.

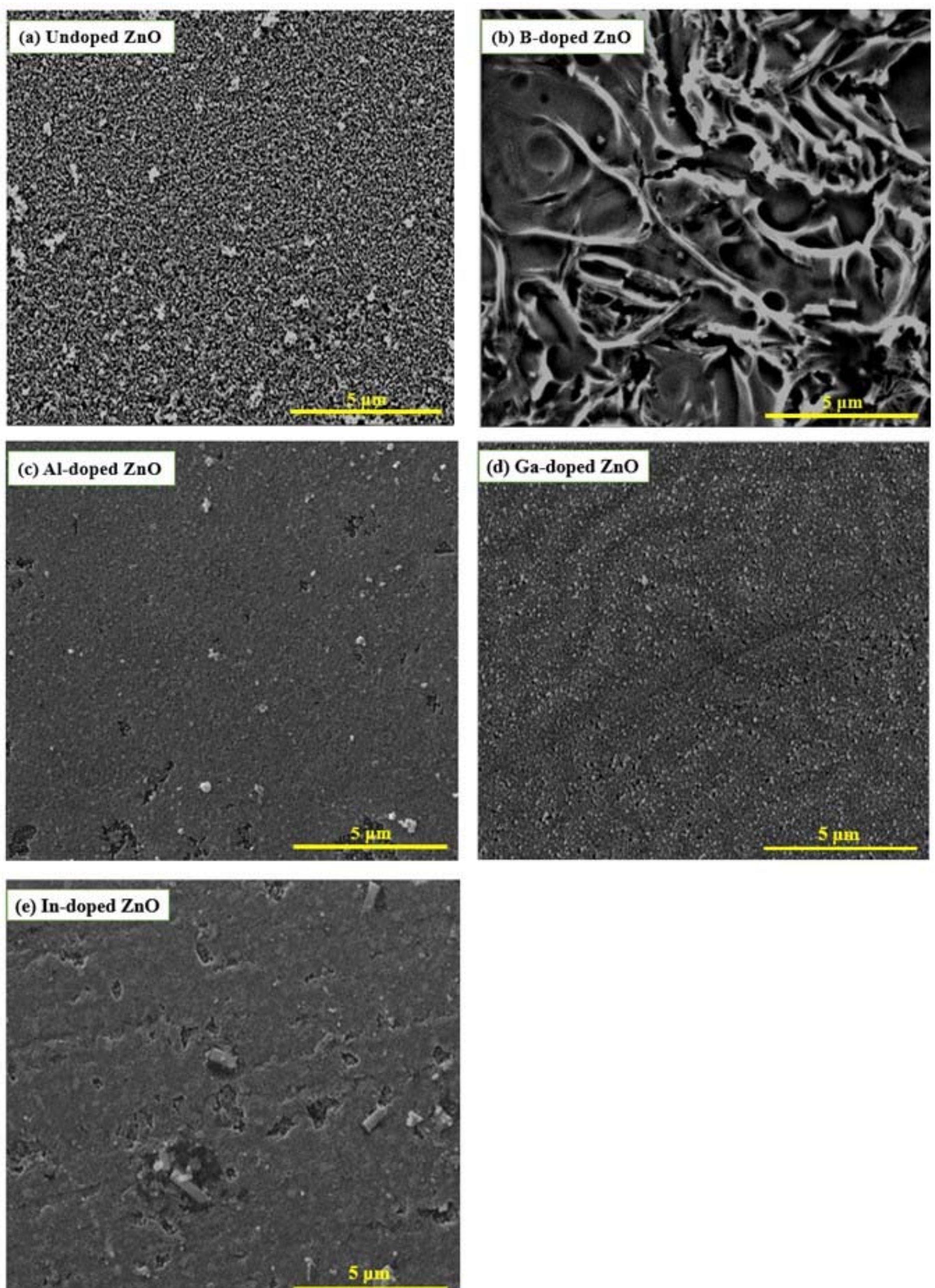

Figure 5. SEM micrographs of (**a**) undoped ZnO, (**b**) B-doped ZnO, (**c**) Al-doped ZnO, (**d**) Ga-doped ZnO, and (**e**) In-doped ZnO thin films.

4. Conclusions

In summary, structural, optical, and morphological properties of dip-synthesized un-doped ZnO and group III elements-doped ZnO (B, Al, Ga, and In) thin films were fabricated at a 3% doping level. Optical characterization of thin films was performed by measuring their transmittance spectra, reflectance spectra, index of refraction, extinction coefficient, optical band gap energy, and other related optical parameters. The transmittance of all investigated thin films was found to attain high values, more than 80% in the visible region. The optical band gap E_g of the undoped ZnO thin film was found to be around 3.27 eV. The E_g values of B-doped ZnO and Ga-doped ZnO were found to decrease with respect to that of undoped ZnO thin films. On the other hand, the E_g values of Al-doped ZnO and In-doped ZnO thin films were found to increase when compared with that of undoped ZnO thin films.

Undoped ZnO thin films exhibited an index of refraction ranging between 1.6 and 2.22, which was very close to that of bulk ZnO. We measured and interpreted nonlinear optical parameters of undoped ZnO and group III elements (B, Al, Ga, and In)-doped ZnO thin films. The drastic change of optical properties of annealed dip-synthesized undoped ZnO thin films upon doping with (B, Al, Ga and In) elements indicated a practical and feasible possibility for tuning optical and electronic properties, in order for the films to be used as key candidate materials for the fabrication of modern optoelectronic and photonic devices at commercial scales. Furthermore, XRD measurements were analyzed and interpreted. We found that undoped ZnO thin films exhibit a hexagonal structure. Moreover, as 3% doping levels of B and In were introduced in ZnO thin films, a structural phase transition was observed that could be attributed to the large difference between the size of B and In atoms compared to the size of Zn atoms. Ga-doped ZnO and Al-doped ZnO thin films were found to preserve the hexagonal structure, as the sizes of Ga and Al atoms are close to that of Zn atoms. Additionally, introducing B and In atoms increased the grain size considerably. On the other hand, introducing Ga and Al atoms decreased the grain size significantly. We investigated the microstructure and the surface morphology of thin films by analyzing and interpreting their SEM micrographs. Our results indicated that undoped ZnO films exhibit a smooth surface with vanishingly small grains of ZnO scattered throughout the surface. SEM micrographs of B-doped ZnO thin films showed coarse features, indicating randomly distributed ice land-like topographies. As Al atoms were introduced, grains became finer and clearer. Micrographs of Ga-doped ZnO thin films indicated small nanoparticles had appeared on the surface. These nanoparticles were refined and softened to form regular nanofeatures. The SEM results of In-doped ZnO thin film showed sheet-like features with few cracks. The SEM results agreed well with the measured XRD patterns of all investigated thin films. Remarkably, significantly tuning the structural, optical, and morphological of doped ZnO thin films should pave the way for designing the next generation of the films' technological device applications.

Author Contributions: Conceptualization, A.M.A., A.A.A., Q.M.A.-B., Z.A. and I.A.Q.; methodology, A.M.A., Q.M.A.-B. and A.A.A.; software, A.M.A. and Q.M.A.-B.; validation, A.M.A., A.A.A., and I.A.Q.; formal analysis, A.M.A., Q.M.A.-B., Z.A. and A.A.A.; investigation, A.M.A., Q.M.A.-B. and A.A.A.; resources, A.M.A. and I.A.Q.; data curation, A.M.A., Q.M.A.-B. and Z.A.; writing—original draft preparation, A.M.A. and Q.M.A.-B.; writing—review and editing, A.M.A., A.A.A. and I.A.Q.; visualization, A.M.A. and Q.M.A.-B.; project administration, A.M.A. and A.A.A.; funding acquisition, A.M.A., A.A.A., Q.M.A.-B.. All authors have read and agreed to the published version of the manuscript.

Funding: This research received no external funding.

Acknowledgments: The authors would like to thank Jordan University of Science and Technology in Jordan for the generous financial and technical support provided by the Deanship of Scientific Research. The authors would like to thank M-Ali Al-Akhras in giving unlimited access to use Biomedical Physics Laboratory.

Conflicts of Interest: The authors declare no conflict of interest. The funders had no role in the design of the study; in the collection, analyses, or interpretation of data; in the writing of the manuscript, or in the decision to publish the results.

References

1. Ko, S.H.; Lee, D.; Kang, H.W.; Nam, K.H.; Yeo, J.Y.; Hong, S.J.; Grigoropoulos, C.P.; Sung, H.J. Nanoforest of hydrothermally grown hierarchical ZnO nanowires for a high efficiency dye-sensitized solar cell. *Nano Lett.* **2011**, *11*, 666–671. [CrossRef] [PubMed]
2. Liu, Y.; Li, Y.; Zeng, H. ZnO-based transparent conductive thin films: Doping, performance, and processing. *J. Nanomater.* **2013**, *2013*. [CrossRef]
3. Gong, H.; Song, H.; Zhang, S.; Ni, K.; Dong, X. An optical liquid level sensor based on polarization-maintaining fiber modal interferometer. *Sens. Actuators A Phys.* **2014**, *205*, 204–207.
4. Azam, A.; Ahmed, F.; Habib, S.S.; Khan, Z.H.; Salah, N.A. Fabrication of Co-doped ZnO nanorods for spintronic devices. *Met. Mater. Int.* **2013**, *19*, 845–850. [CrossRef]
5. Kolhe, P.S.; Shinde, A.B.; Kulkarni, S.; Maiti, N.; Koinkar, P.M.; Sonawane, K.M. Gas sensing performance of Al doped ZnO thin film for H2S detection. *J. Alloys Compd.* **2018**, *748*, 6–11.

6. Sahay, P.; Nath, R. Al-doped zinc oxide thin films for liquid petroleum gas (LPG) sensors. *Sens. Actuators B Chem.* **2008**, *133*, 222–227. [CrossRef]
7. Karpina, V.A.; Lazorenko, V.I.; Lashkarev, C.V.; Dobrowolski, V.D.; Kopylova, L.I.; Baturin, V.A.; Pustovoytov, S.A.; Karpenko, A.J.; Eremin, S.A.; Lytvyn, P.M.; et al. Zinc oxide–analogue of GaN with new perspective possibilities. *Cryst. Res. Technol.* **2004**, *39*, 980–992. [CrossRef]
8. Asl, H.Z.; Rozati, S.M. High-Performance Spray-Deposited Indium Doped ZnO Thin Film: Structural, Morphological, Electrical, Optical, and Photoluminescence Study. *J. Electron. Mater.* **2018**, *47*, 3568–3576. [CrossRef]
9. Gonçalves, R.; Barrozo, P.; Brito, G.; Viana, B.; Cunha, F. The effect of thickness on optical, structural and growth mechanism of ZnO thin film prepared by magnetron sputtering. *Thin Solid Film* **2018**, *661*, 40–45. [CrossRef]
10. Liang, W.; Yoffe, A. Transmission spectra of ZnO single crystals. *Phys. Rev. Lett.* **1968**, *20*, 59. [CrossRef]
11. Park, Y.; Litton, C.; Collins, T.; Reynolds, D. Exciton spectrum of ZnO. *Phys. Rev.* **1966**, *143*, 512. [CrossRef]
12. Potter, D.B.; Powell, M.J.; Parkin, I.P.; Carmalt, C.J. Aluminium/gallium, indium/gallium, and aluminium/indium co-doped ZnO thin films deposited via aerosol assisted CVD. *J. Mater. Chem. C* **2018**, *6*, 588–597. [CrossRef]
13. Kumar, V.; Singh, R.; Purohit, L.; Mehra, R. Structural, transport and optical properties of boron-doped zinc oxide nanocrystalline. *J. Mater. Sci. Technol.* **2011**, *27*, 481–488. [CrossRef]
14. Wen, B.; Liu, C.Q.; Wang, N.; Wang, H.L.; Liu, S.M.; Jiang, W.W.; Ding, W.Y.; Fei, W.D.; Chai, W.P. Crystallization Behavior and Properties of B-Doped ZnO Thin Films Prepared by Sol-Gel Method with Different Pyrolysis Temperatures. *Chin. J. Chem. Phys.* **2016**, *29*, 229–233. [CrossRef]
15. Wong, L.H.; Lai, Y.S. Characterization of boron-doped ZnO thin films prepared by magnetron sputtering with (100− x) ZnO–xB 2 O 3 ceramic targets. *Thin Solid Film* **2015**, *583*, 205–211. [CrossRef]
16. Djelloul, A.; Larbah, Y.; Adnane, M.; Labdelli, B.; Ziane, M.; Manseri, A.; Messaoud, A. Properties of Undoped and (Al, In) Doped ZnO Thin Films Prepared by Ultrasonic Spray Pyrolysis for Solar Cell Applications. *J. Nano Electron. Phys.* **2018**, *10*, 02036-1–02036-5. [CrossRef]
17. Varghese, J.; Aswathy, N.; Saji, S.D.; Vinodkumar, R. Structural and optical modification of ZnO: Al thin films by molybdenum co-doping and the origin of green emission. *AIP Conf. Proc.* **2018**, *1953*, 030079.
18. Serrao, F.J.; Sandeep, K.; Bhat, S.; Dharmaprakash, S. High energy electron irradiation effects on Ga-doped ZnO thin films for optoelectronic space applications. *Appl. Phys. A* **2018**, *124*, 224. [CrossRef]
19. Kayani, Z.N.; Yaseen, N.; Riaz, S.; Naseem, S. Investigation of Fe doping on the magnetic and optical properties of ZnO thin films. *Mater. Res. Express* **2018**, *5*, 036418. [CrossRef]
20. Jo, G.H.; Kim, S.-H.; Koh, J.-H. Enhanced electrical and optical properties based on stress reduced graded structure of Al-doped ZnO thin films. *Ceram. Int.* **2018**, *44*, 735–741. [CrossRef]
21. Lee, C.-S.; Yoon, K.-H.; Ahn, B. Improved optical transmittance of boron doped ZnO thin films by low pressure chemical vapor deposition with pulse boron doping. *J. Electrochem. Soc.* **2011**, *158*, H482–H486. [CrossRef]
22. Wen, B.; Liu, C.Q.; Wang, N.; Wang, H.L.; Liu, S.M.; Jiang, W.W.; Ding, W.Y.; Fei, W.D.; Chai, W.P. Properties of boron-doped ZnO thin films deposited by pulsed DC magnetron sputtering at different substrate temperatures. *Appl. Phys. A* **2015**, *121*, 1147–1153. [CrossRef]
23. Kaur, G.; Mitra, A.; Yadav, K. Pulsed laser deposited Al-doped ZnO thin films for optical applications. *Prog. Nat. Sci. Mater. Int.* **2015**, *25*, 12–21. [CrossRef]
24. Tsin, F.; Venerosy, A.; Vidal, J.; Collin, S.; Clatot, J.; Lombez, L.; Paire, M.; Borensztajn, S.; Broussillou, C.; Grand, P.-P. Electrodeposition of ZnO window layer for an all-atmospheric fabrication process of chalcogenide solar cell. *Sci. Rep.* **2015**, *5*, 1–8. [CrossRef] [PubMed]
25. Kim, S.; Yoon, H.; Kim, D.Y.; Kim, S.-O.; Leem, J.-Y. Optical properties and electrical resistivity of boron-doped ZnO thin films grown by sol–gel dip-coating method. *Opt. Mater.* **2013**, *35*, 2418–2424. [CrossRef]
26. Al Sanableh, A. Structural and Optical Properties of ZnO Thin Films Deposited by Sol Gel Caoting Technique. Master's Thesis, Jordan Univesity of Science and Technology Irbid, Physics Department, Irbid, Jordan, 2006.
27. Ahmad, A.; Alsaad, A.; Al-Bataineh, Q.; Al-Naafa, M. Optical and structural investigations of dip-synthesized boron-doped ZnO-seeded platforms for ZnO nanostructures. *Appl. Phys. A* **2018**, *124*, 458. [CrossRef]
28. Lee, J.-H.; Park, B.-O. Transparent conducting ZnO: Al, In and Sn thin films deposited by the sol–gel method. *Thin Solid Film* **2003**, *426*, 94–99. [CrossRef]

29. Ahmad, A.; Alsaad, A.; Al-Bataineh, Q.; Bani-Salameh, A.; Al-Khateeb, H.; Al-Naafa, M. Optical and Structural Characterization of Dip Synthesized Al-B Co-doped ZnO Seeded Platforms for ZnO Nanostructures. *Jordan J. Phys.* **2017**, *10*, 33–48.
30. Schropp, R.E.; Zeman, M. Amorphous and microcrystalline silicon solar cells: Modeling, materials and device technology. *Springer* **1998**, *8*. [CrossRef]
31. Ellipsometry, S.; Boccara, A.C.; Pickering, C.; Rivory, J. (Eds.) *Proceedings of the First International Conference on Spectroscopic Ellipsometry*; Elsevier: Amsterdam, The Netherlands, 1993.
32. Jellison, G., Jr. Data analysis for spectroscopic ellipsometry. *Thin Solid Film* **1993**, *234*, 416–422. [CrossRef]
33. Jellison, G., Jr.; Chisholm, M.; Gorbatkin, S. Optical functions of chemical vapor deposited thin-film silicon determined by spectroscopic ellipsometry. *Appl. Phys. Lett.* **1993**, *62*, 3348–3350. [CrossRef]
34. Jellison, G.; Boatner, L.; Lowndes, D.; McKee, R.; Godbole, M. Optical functions of transparent thin films of $SrTiO_3$, $BaTiO_3$, and SiOx determined by spectroscopic ellipsometry. *Appl. Opt.* **1994**, *33*, 6053–6058. [CrossRef] [PubMed]
35. Hassanien, A.S.; Akl, A.A. Influence of composition on optical and dispersion parameters of thermally evaporated non-crystalline $Cd_{50}S_{50-x}Se_x$ thin films. *J. Alloys Compd.* **2015**, *648*, 280–290. [CrossRef]
36. Hassanien, A.; Akl, A.A. Effect of Se addition on optical and electrical properties of chalcogenide CdSSe thin films. *Superlattices Microstruct.* **2016**, *89*, 153–169. [CrossRef]
37. Appani, S.K.; Rayapati, S.V.; Sutar, D.; Major, S. Study of transparent conducting Ga-doped ZnO films grown by reactive co-sputtering of Zn and GaAs. *AIP Conf. Proc.* **2018**, *1942*, 120009.
38. Salem, M.; Akir, S.; Ghrib, T.; Daoudi, K.; Gaidi, M. Fe-doping effect on the photoelectrochemical properties enhancement of ZnO films. *J. Alloys Compd.* **2016**, *685*, 107–113. [CrossRef]
39. Kafle, B.; Acharya, S.; Thapa, S.; Poudel, S. Structural and optical properties of Fe-doped ZnO transparent thin films. *Ceram. Int.* **2016**, *42*, 1133–1139. [CrossRef]
40. Khan, S.A.; Al-Hazmi, F.; Al-Heniti, S.; Faidah, A.; Al-Ghamdi, A. Effect of cadmium addition on the optical constants of thermally evaporated amorphous Se–S–Cd thin films. *Curr. Appl. Phys.* **2010**, *10*, 145–152. [CrossRef]
41. Urbach, F. The long-wavelength edge of photographic sensitivity and of the electronic absorption of solids. *Phys. Rev.* **1953**, *92*, 1324. [CrossRef]
42. El-Hagary, M.; Emam-Ismail, M.; Shaaban, E.; El-Taher, A. Effect of γ-irradiation exposure on optical properties of chalcogenide glasses Se70S30−xSbx thin films. *Radiat. Phys. Chem.* **2012**, *81*, 1572–1577. [CrossRef]
43. Parmar, R.; Kundu, R.; Punia, R.; Aghamkar, P.; Kishore, N. Iron modified structural and optical spectral properties of bismuth silicate glasses. *Phys. B Condens. Matter* **2014**, *450*, 39–44. [CrossRef]
44. Melsheimer, J.; Ziegler, D. Band gap energy and Urbach tail studies of amorphous, partially crystalline and polycrystalline tin dioxide. *Thin Solid Film* **1985**, *129*, 35–47. [CrossRef]
45. Ikhmayies, S.J.; Ahmad-Bitar, R.N. A study of the optical bandgap energy and Urbach tail of spray-deposited CdS: In thin films. *J. Mater. Res. Technol.* **2013**, *2*, 221–227. [CrossRef]
46. Aly, K.; Elnaeim, A.A.; Uosif, M.; Abdel-Rahim, O. Optical properties of Ge–As–Te thin films. *Phys. B Condens. Matter* **2011**, *406*, 4227–4232. [CrossRef]
47. Askari, M.; Soltani, N.; Saion, E.; Yunus, W.M.M.; Erfani, H.M.; Dorostkar, M. Structural and optical properties of PVP-capped nanocrystalline $Zn_xCd_{1-x}S$ solid solutions. *Superlattices Microstruct.* **2015**, *81*, 193–201. [CrossRef]
48. Xing, C.; Zhang, Y.; Yan, W.; Guo, L. Band structure-controlled solid solution of Cd1-xZnxS photocatalyst for hydrogen production by water splitting. *Int. J. Hydrog. Energy* **2006**, *31*, 2018–2024. [CrossRef]
49. Eloy, J. *Power Lasers, National School of Physics, Grenoble, France*; John Wiley and Sons: Somerset, NJ, USA, 1984.
50. Sutcliffe, B.T.; Wilson, S. Potential energy curves and surfaces. *Handb. Mol. Phys. Quantum Chem.* **2003**, 574–587.
51. Wemple, S.; DiDomenico, M., Jr. Behavior of the electronic dielectric constant in covalent and ionic materials. *Phys. Rev. B* **1971**, *3*, 1338. [CrossRef]
52. Fu, D.W.; Zhang, W.; Cai, H.L.; Ge, J.Z.; Zhang, Y.; Xiong, R.G. Diisopropylammonium chloride: A ferroelectric organic salt with a high phase transition temperature and practical utilization level of spontaneous polarization. *Adv. Mater.* **2011**, *23*, 5658–5662. [CrossRef]

53. Girisun, T.S.; Dhanuskodi, S. Linear and nonlinear optical properties of tris thiourea zinc sulphate single crystals. *Cryst. Res. Technol. J. Exp. Ind. Crystallogr.* **2009**, *44*, 1297–1302. [CrossRef]
54. El Radaf, I. Structural, optoelectrical, linear, and nonlinear optical characterizations of the $Cu_2ZnGeSe_4$ thin films. *J. Mater. Sci. Mater. Electron.* **2020**, *31*, 3228–3237. [CrossRef]
55. Kumarasinghe, P.; Dissanayake, A.; Pemasiri, B.; Dassanayake, B. Effect of post deposition heat treatment on microstructure parameters, optical constants and composition of thermally evaporated CdTe thin films. *Mater. Sci. Semicond. Process.* **2017**, *58*, 51–60. [CrossRef]
56. Islam, M.; Huda, Q.; Hossain, M.; Aliyu, M.; Karim, M.; Sopian, K.; Amin, N. High quality 1 μm thick CdTe absorber layers grown by magnetron sputtering for solar cell application. *Curr. Appl. Phys.* **2013**, *13*, S115–S121. [CrossRef]
57. Enriquez, J.P.; Mathews, N.; Hernández, G.P.; Mathew, X. Influence of the film thickness on structural and optical properties of CdTe thin films electrodeposited on stainless steel substrates. *Mater. Chem. Phys.* **2013**, *142*, 432–437. [CrossRef]
58. Eid, A.; Seddek, M.; Salem, A.; Dahy, T. Structural characterization and optical properties of $Cd_{(1-x)}Mn_xSe$ thin films. *Vacuum* **2008**, *83*, 401–407. [CrossRef]
59. Caglar, Y. Sol–gel derived nanostructure undoped and cobalt doped ZnO: Structural, optical and electrical studies. *J. Alloys Compd.* **2013**, *560*, 181–188. [CrossRef]
60. Barrett, C.; Massalski, T. Structure of Metals: Crystallographic Methods. Available online: https://www.amazon.com/Structure-Metals-Third-Crystallographic-International/dp/0080261728 (accessed on 26 March 2020).
61. Ramırez-Ortiz, J.; Ogura, T.; Medina-Valtierra, J.; Acosta-Ortiz, S.E.; Bosch, P.; de Los Reyes, J.A.; Lara, V.H. A catalytic application of Cu_2O and CuO films deposited over fiberglass. *Appl. Surf. Sci.* **2001**, *174*, 177–184. [CrossRef]
62. Li, J.; Li, H.; Xue, Y.; Fang, H.; Wang, W. Facile electrodeposition of environment-friendly Cu_2O/ZnO heterojunction for robust photoelectrochemical biosensing. *Sens. Actuators B Chem.* **2014**, *191*, 619–624. [CrossRef]
63. Habubi, N.; Oboudi, S.; Chiad, S. Study of some optical properties of mixed SnO_2-CuO thin films. *J. Nano-Electron. Phys.* **2012**, *4*, 04008.
64. Mott, N.F.; Davis, E.A. *Electrical Process in Non-Crystalline Materials*; Clarendon: Oxford, UK, 1979.
65. The International Union of Crystallography is a Non-Profit Scientific Union Serving the World-Wide Interests of Crystallographers and Other Scientists Employing Crystallographic Methods. Available online: https://www.iucr.org/resources/other-directories/software/powderx (accessed on 22 March 2020).
66. Znaidi, L. Sol–gel-deposited ZnO thin films: A. review. *Mater. Sci. Eng. B* **2010**, *174*, 18–30. [CrossRef]
67. Takahashi, Y.; Kanamori, M.; Kondoh, A.; Minoura, H.; Ohya, Y. Photoconductivity of ultrathin zinc oxide films. *Jpn. J. Appl. Phys.* **1994**, *33*, 6611. [CrossRef]
68. Lee, H.; Lee, J.; Kim, T.; Kim, D.; Cho, W. Formation mechanism of preferential c-axis oriented ZnO thin films grown on p-Si substrates. *J. Mater. Sci.* **2004**, *39*, 3525–3528. [CrossRef]
69. Xu, L.; Li, X.; Chen, Y.; Xu, F. Structural and optical properties of ZnO thin films prepared by sol–gel method with different thickness. *Appl. Surf. Sci.* **2011**, *257*, 4031–4037. [CrossRef]
70. Tsai, D.-C.; Chang, Z.-C.; Kuo, B.-H.; Wang, Y.-H.; Chen, E.-C.; Shieu, F.-S. Thickness dependence of the structural, electrical, and optical properties of amorphous indium zinc oxide thin films. *J. Alloys Compd.* **2018**, *743*, 603–609. [CrossRef]
71. Sandeep, K.; Bhat, S.; Dharmaprakash, S. Nonlinear absorption properties of ZnO and Al doped ZnO thin films under continuous and pulsed modes of operations. *Opt. Laser Technol.* **2018**, *102*, 147–152. [CrossRef]
72. Hadimani, P.; Ghosh, S.; Sil, A. Preparation of Fe doped ZnO thin films and their structural, magnetic, electrical characterization. *Superlattices Microstruct.* **2018**, *120*, 199–208. [CrossRef]
73. Ivanova, T.; Harizanova, A.; Koutzarova, T.; Vertruyen, B.; Stefanov, B. Structural and morphological characterization of sol-gel ZnO: Ga films: Effect of annealing temperatures. *Thin Solid Film* **2018**, *646*, 132–142. [CrossRef]
74. Sarma, H.; Sarma, K. X-ray Peak Broadening Analysis of ZnO Nanoparticles Derived by Precipitation method. *Int. J. Sci. Res. Publ.* **2014**, *4*, 1–7.
75. Ramakanth, K. *Basics of X-ray Diffraction and its Application*; I K International Publishing House Pvt. Ltd.: New Delhi, India, 2007.

76. Khan, Z.R.; Khan, M.S.; Zulfequar, M.; Khan, M.S. Optical and structural properties of ZnO thin films fabricated by sol-gel method. *Mater. Sci. Appl.* **2011**, *2*, 340–345. [CrossRef]
77. Horiuchi, S.; Tokunaga, Y.; Giovannetti, G.; Picozzi, S.; Itoh, H.; Shimano, R.; Kumai, R.; Tokura, Y. Above-room-temperature ferroelectricity in a single-component molecular crystal. *Nature* **2010**, *463*, 789–792. [CrossRef] [PubMed]

© 2020 by the authors. Licensee MDPI, Basel, Switzerland. This article is an open access article distributed under the terms and conditions of the Creative Commons Attribution (CC BY) license (http://creativecommons.org/licenses/by/4.0/).